PROCEEDINGS, TOUGH Symposium 2006
Lawrence Berkeley National Laboratory, Berkeley, California, May 15–17, 2006

TOUGH2/ITOUGH2 ANALYSIS OF THE GAS MIGRATION TEST (GMT) AT THE GRIMSEL TEST SITE (SWITZERLAND)

Rainer Senger[1], Bill Lanyon[2], Paul Marschall[3], Stratis Vomvoris[3], Ai Fujiwara[4]

[1]Intera Incorporated, 9111A Research Blvd., Austin, Texas 78757, rsenger@intera.com
[2]Fracture Systems Ltd, Tregurrian, St Ives, Cornwall, UK, bill@fracture-systems.co.uk
[3]NAGRA, Hardstrasse 73, CH-5430 Wettingen, Switzerland, paul.marschall@nagra.ch
[4]RWMC, N0.15 Mori Bldg.,2-8-10,Toranomon,Minato-ku,Tokyo,Japan, ai-fujiwara@rwmc.or.jp

ABSTRACT

The Gas Migration Test (GMT) at the Grimsel Test Site (GTS) underground laboratory in central Switzerland was designed to investigate gas migration through an engineered barrier system (EBS). The EBS consists of a concrete silo embedded in a sand/bentonite buffer emplaced in a silo cavern that intersects a shear zone in the surrounding granite host rock. The experiment was performed in a series of stages: (1) excavation of the access drift and silo cavern, (2) construction and instrumentation, (3) saturation of the EBS, (4) water tests, (5) long-term gas injection at different rates, (6) post-gas water testing, (7) gas injection with a "cocktail" of gas tracers, and (8) depressurization and dismantling.

A numerical model of the GMT was implemented with the two-phase flow code TOUGH2, representing the GMT silo with a multi-layered radially-symmetric mesh and the surrounding water-conducting granite shear zone with a 2D vertical feature. The different stages of the experiment were simulated in sequence using the results of the previous stage as initial conditions for the subsequent stage. Two-phase flow parameters for the EBS were derived from laboratory experiments on core samples of the different materials that comprise the EBS, while hydraulic properties of the sand/bentonite and of relevant interface zones were calibrated to the pressure responses in the silo and selected piezometers in the sand/bentonite. The results of the numerical modeling of the GMT experiment show that the main features and processes of the different stages of the experiment could be reasonably well reproduced. In addition to standard two-phase flow processes, inferred coupled hydromechanical phenomena were implemented using pressure-dependent permeability relationships on interfaces at the top of the silo and between the sand/bentonite and the granite host rock. Changes in the hydraulic properties of the sand/bentonite that occurred during the different test stages were incorporated by updating material properties for the simulation of the test stages. Time-dependent permeability relationships were calibrated for the tunnel seal to account for the gradual decrease in water inflow from the upper cavern into the access tunnel and the drift.

INTRODUCTION

The GMT was conducted at the Grimsel Test Site (GTS) underground laboratory operated by the National Cooperative for the Disposal of Radioactive Waste (NAGRA) in central Switzerland (Shimura et al, 2006). The GMT experiment is operated by NAGRA and Obayashi Corporation under the leadership of the Japanese Radioactive Waste Management Funding and Research Center (RWMC). In addition to the GMT experiment team, subtask partners contributed to the experiment by conducting gas tracer tests (GRS, Germany) and modeling studies using coupled two-phase geomechanical codes (ANDRA, France, BGR, Germany, and ENRESA, Spain).

The detailed geometry of the EBS, consisting of the concrete silo, gas vent, sand/bentonite layers, and surrounding host rock, was incorporated in a numerical model as shown in Figure. 1. The model was implemented with TOUGH2 (Pruess, 1991) using a radially symmetric mesh geometry for the EBS and a 2D cross sectional mesh representing the shear-zone of the surrounding granite host rock. The effect of the access tunnel was accounted for by 2D cross-sectional elements representing the 2-m thick tunnel seal that separates the GMT silo from the atmospheric conditions in the access tunnel (Fig. 1).

The sand/bentonite buffer material consisting of 20% bentonite (Kunigel V1) and 80% sand (by weight) was emplaced as a series of lifts, typically 6-9 cm thick after compaction at an in-situ density of about 1.8 g/cm^2 and a water content of 11% (water saturation of about 70%). Instrumentation was arranged by layers (made up of between 3 and 9 lifts). The sand/bentonite in Layers 8 to 10 (see Fig. 1) was mixed with a lead-nitrate solution (for gas flow-path visualization), which resulted in reduced swelling of the bentonite. These sand/bentonite layers were represented in the model by multiple element rows with the top row corresponding to the top lift in Layers 8 – 10.

Initial estimates of hydraulic and two-phase properties were obtained from laboratory studies of sand/bentonite material (Romero et al., 2003, Romero

and Castellanos, 2004), and geosphere characterization at the GMT site.

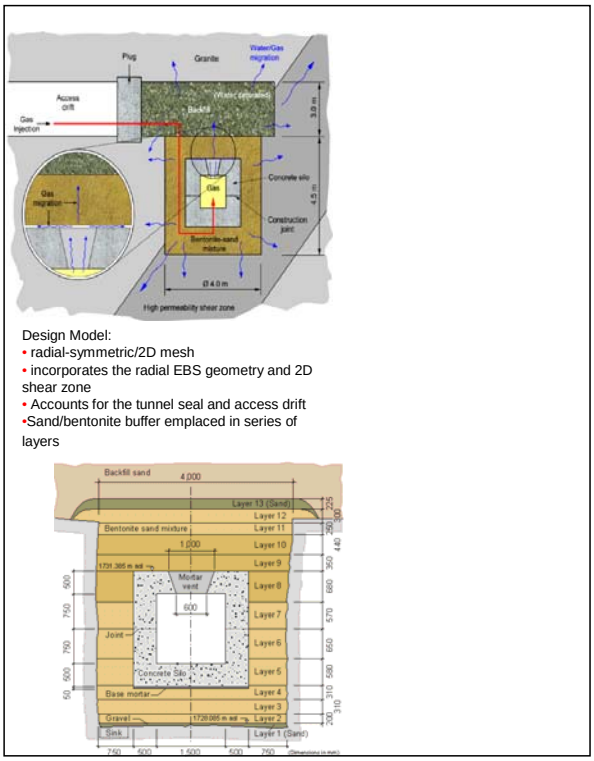

Figure 1. GMT geometry and model design

The lead-nitrate solution added to the sand/bentonite during emplacement of Layers 8-10 (Fig. 1) caused reduced swelling of the bentonite and a correspondingly higher permeability compared to the untreated sand/bentonite (S/B) in Layers 2 – 7 and 11 – 12 (Romero and Castellanos, 2004). The sand/bentonite/ lead nitrate buffer material (S/B/Pb) also showed lower capillary pressures and different relative permeabilities compared to the untreated S/B samples. The properties for the different materials are summarized in Tables 1 and 2.

The entire GMT involved a series of experimental stages over a six year period starting in 1998: (1) excavation of the access drift and silo cavern, (2) construction and instrumentation, (3) saturation of the EBS by natural water inflow and water injection (ca. 12 months), (4) water testing (WT1) that included constant-rate injection (RI) and withdrawal (RW) and sinusoidal withdrawal (RWSin) from the silo, sinusoidal injection tests (CVRISin) in the the upper cavern, and a withdrawal test (WL1) from Layer 1 (4 months), (5) gas injection at different rates (RGI1-3b) into the concrete silo (8 months), (6) post-gas water testing (WT2, 3 months), (7) second gas injection phase (RGI4a-b) (3 months), (8) depressurization and dewatering, and (9) EBS excavation and characterization.

Table 1. Summary of initial hydraulic properties

		Hydraulic Properties		
Unit	TOUGH2 Material	Permeability k (m^2)	Porosity ϕ	Pore Compressibility $C_p(Pa^{-1})$
Granite (fracture)	GRANF	5.E-17	0.01	3.4E-8
Granite (DRZ)	GRDRZ	1.65E-16	0.01	3.4E-8
Granite (interface)	GRINT	2.5E-14	0.01	0.
Gravel (bot. Drain)	GRDRN	1.E-12	0.3	3.3E-8
Concrete	LINCR	1.E-18	0.2	1.35E-10
Tunnel fill/sand	TFILL	1.E-12	0.32	7.71E-9
Silo backfill	BACKF	1.E-12	0.32	7.5E-10
Gas vent	GVENT	1.E-13	0.3	3.3.E-10
Tunnel seal	TSEAL	2.32E-15	0.1	2.7E-10
Shear zone path	GRCON	7.5E-14	0.01	0.
SAND/BENTONITE				
Layers 2 – 6, 11-12	BENTS	2.22E-19	0.3	3.3.E-8
Layer 7	BSLA7	K_x =5.E-18 K_z =1.E-18	0.3	3.3.E-8
Sand/Bent. Interface	BENTI	K_x =1.E-18 K_z =5.E-18	0.3	3.3E-8
Layers 8 – 10	BS810	K_x =2.46E-16 K_z =2.46E-17	0.3	2.5E-8
Top Layer 8	BSTOP	K =5.0E-16	0.3	2.5E-8

Table 2. Summary of two-phase flow parameters

	Two-Phase Flow Properties				
TOUGH2 Material	TPF Model P_c/k_r	Air-Entry Pressure P_{ae}(Pa)	Shape Parameter[1] P_c/k_r	Residual Water Sat. S_{lr} {P_c/k_r}	Resid. Gas Sat. S_{gr}
GRANF	vG/*vG*	1.E+5	n=1.88/*1.88*	0.1/*0.1*	0.01
GRDRZ	vG/*vG*	5.E+4	n=1.88/*1.88*	0.1/*0.1*	0.01
GRINT	vG/*vG*	1.E+4	n=1.88/*1.88*	0.1/*0.1*	0.01
GRDRN	vG/*vG*	5.E+2	n=*2*/*2*	0.1/*0.1*	0.01
LINCR	vG/*vG*	1.E+6	n=*2*/*2*	0.25/*0.25*	0.01
TFILL	vG/*vG*	500.	n=*2*/*2*	0.25/*0.25*	0.01
BACKF	vG/*vG*	500.	n=*2*/*2*	0.25/*0.25*	
GVENT	vG/*vG*	500.	n=*2*/*2*	0.3/*0.3*	0.01
TSEAL	vG/*vG*	100.	n=*2*/*2*	0.25/*0.25*	0.01
GRCON	vG/vG	100.	n=1.88/*1.88*	0.1/*0.1*	0.01
SAND/BENT					
BENTS	vG/*Grant*	4.E+4	n=2.5/λ=*2*	0.58/*0.3*	0.01
BSLA7	vG/*Grant*	1.E+4	n=2.5/λ=*2*	0.58/*0.3*	0.01
BENTI	vG/*Grant*	1.E+4	n=2.5/λ=*2*	0.58/*0.3*	0.01
BS810/BSTOP	vG/*BC*	3.E+3	n=1.2/λ=*0.5*	0.35/*0.5*	0.01

The pressure responses in selected sensors and the injection rates during the GMT starting with the saturation stage 3 are shown in Figure 2. The saturation stage started with water injection in Layer 1 at a relatively low rate, followed at the by water injection into the upper cavern (Layer 13) in mid 2001 (Fig. 2). Fluctuations in the cavern injection rate (FlowL13/2) cause significant pressure responses in the upper cavern (PI/13/Plug) and in the S/B/Pb Layers 8-10, whereas the lower permeability S/B Layers 3-5 indicate only a gradual and a significantly delayed response to the pressurization of the upper cavern. The overall trend of the water injection indicates a decreasing rate whereas the cavern pressure increases prior to the gas injection phase (RGI1-RGI3). Following this first gas injection phase, the water injection rate was reduced to lower the upper cavern pressure to the level prior to gas injection. The individual gas injection steps produce distinct increases in the silo pressure (PI/7/9/0) and lesser but noticeable responses in S/B/Pb Layers 8-10. At the start of RGI3b, the pressure in the lower permeability S/B layer (PI/5/4/3) shows a steep increase, whereas the pressures in Layer 3 indicate a more delayed response (PI/3/8/1).

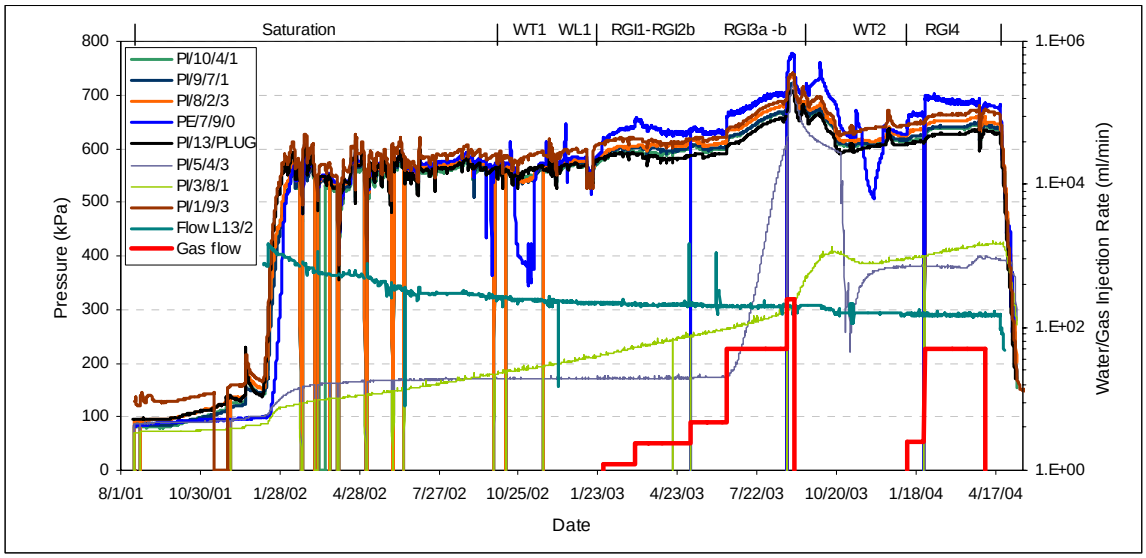

Figure 2. Measured pressures and injection rates during the GMT (PI/z/x/y indicates the transducer location in Layer 'z' and 'y' corresponds to the max. radial distances: '0'=0.m, '1' <0.75m,' 2'<1.25m,'3'<1.5m).

TOUGH2/ITOUGH2 MODEL RESULTS

During the GMT experiment, the individual stages were simulated for prediction of the expected pressure and saturation responses. Subsequent analyses of the observed pressure responses for an individual stage were used to update and refine the model. In several cases, later stages of the experiment revealed information requiring updating the model and revising the simulations of preceding experimental stages. The simulations started with undisturbed conditions in the granite host rock affected by the main drift of the GTS, followed by the cavern excavation and construction of the GMT silo. Modeling results for the main phases of the experiment were compared with those from the subtask partners, including results from fully coupled hydromechanical models, during annual review meetings. For the TOUGH2 model, potential geomechanical phenomena observed during the GMT were implemented using pressure-dependent and time-dependent permeability functions.

Saturation of the EBS

The saturation phase of the GMT experiment started with water injection into Layer 1 in August 2001, followed by water injection into Layer 13 in the upper cavern from September 2001 to September 2002. Once the upper cavern was pressurized, the water injection rate was adjusted to maintain an approximately constant pressure of about 560 kPa in Layer 13 (PI/13/Plug). The simulation of the saturation phase provided a limited calibration of the sand/bentonite properties, given in Table 1, which reproduced reasonably well the overall pressure and saturation response in the different sand/bentonite layers, as presented in detail in Senger et al. (2005).

The calibration indicated reduced permeability of the S/B layers by a factor of two from the laboratory data and intermediate permeability for Layer 7 between the low permeability S/B and the higher permeability S/B/Pb Layers (Fig. 1). Moreover, the simulation of the pressure-response in the silo suggested a higher-permeable interface at the top of the Layer 8. The simulation results in near full saturation of the S/B/Pb layers, whereas the S/B layers remain partially saturated, as shown in the simulated distribution of gas saturation and pressure at the end of the saturation phase (Fig. 3).

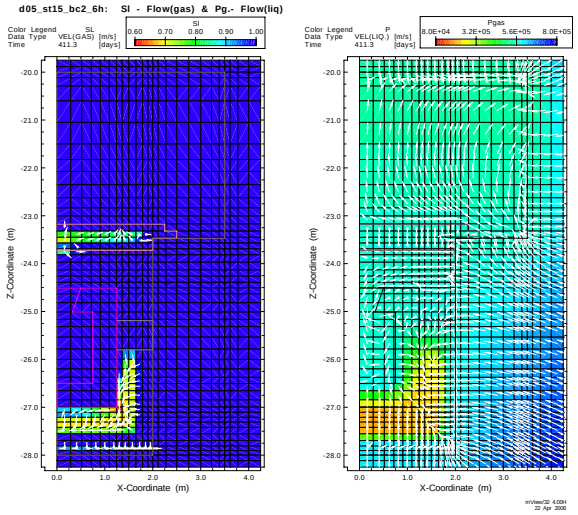

Figure 3 Simulated distribution of gas saturation and gas flow (left) and pressure and water flow (right) at the end of saturation.

Water Test 1 (WT1) and WL1 Test

WT1 was designed to quantify the overall hydraulic characteristics of the sand/bentonite buffer following saturation and to identify potential interfaces along the concrete silo and along the granite rock. In addition the hydraulic communication between the concrete silo, Layer 1, and the upper cavern was tested by the water test in Layer 1 (WL1).

The pressure in the upper cavern (PI/13/Plug) is controlled largely by the prescribed water injection into the upper cavern which had to be gradually reduced to maintain approximately constant cavern pressures of about 560 kPa (Fig. 2). This suggested a gradual decrease in the permeability of the drainage elements (tunnel seal) corresponding to the observed decline in outflow from the upper cavern through the plug and shear zone. This observed decrease in outflow was implemented in the model by calibrating a time-dependent decrease in the permeability of the tunnel seal during WT1 – WL1.

Inverse modeling of WT1 was performed to estimate the hydraulic properties for the S/B/Pb layers (i.e., permeabilities k_x, k_z, and compressibility C_p) and to better characterize the potential interface zones (BSTOP and GRINT) (Fig. 1). For this, initial estimate of permeability for both BS810 and BSTOP was the same in the inverse simulation. All other hydraulic parameters and two-phase flow properties were as given in Tables 1 and 2. The effect of a stress-dependent permeability for BSTOP was also tested in a separate inverse simulation implementing a pressure-dependent permeability function.

The inverse simulations shows that the overall WT1 response could be reasonably well reproduced assuming a constant permeability of BSTOP, calibrating to the silo pressure (PE/7/9/0) as measured pressures in S/B/Pb Layers 8-10 (Fig. 4). The inverse simulation assuming a pressure-dependent permeability produced similar results (Senger, 2005), both reproducing the distinct pressure decline in Layers 8 – 10 during RW1. The main difference between the two cases was in the silo pressure response. Whereas the case with pressure dependent permeability of BSTOP reproduced well the RW1 sequence and the individual recovery sequences, the pressure buildup for RI1 and RI2 were noticeably underestimated. The results assuming a constant permeability of BSTOP better reproduced the pressure buildup for RI1 and RI2, but showed an offset in the silo pressure during the recovery periods of the individual test sequences compared to the cavern pressure (Fig. 4). This could possibly be due to an instrumentation offset.

The simulated pressure increase during RI1 is noticeably greater than the observed pressure buildup, but is comparable with that measured for RI2 (Fig. 4). This suggested an overall decrease in the S/B/Pb permeability above the silo between RI1 and RI2 which could be a non-linear response to stress changes during RW1 The inverse modeling provided estimates for horizontal and vertical permeability of BS810 (Fig. 4) that are lower than those in Table 1. The permeability of the interface layer at the top of Layer 8 (BSTOP) is slightly higher (3.2E-16 m^2) compared to the horizontal permeability of BS810 (1.7E-16 m^2).

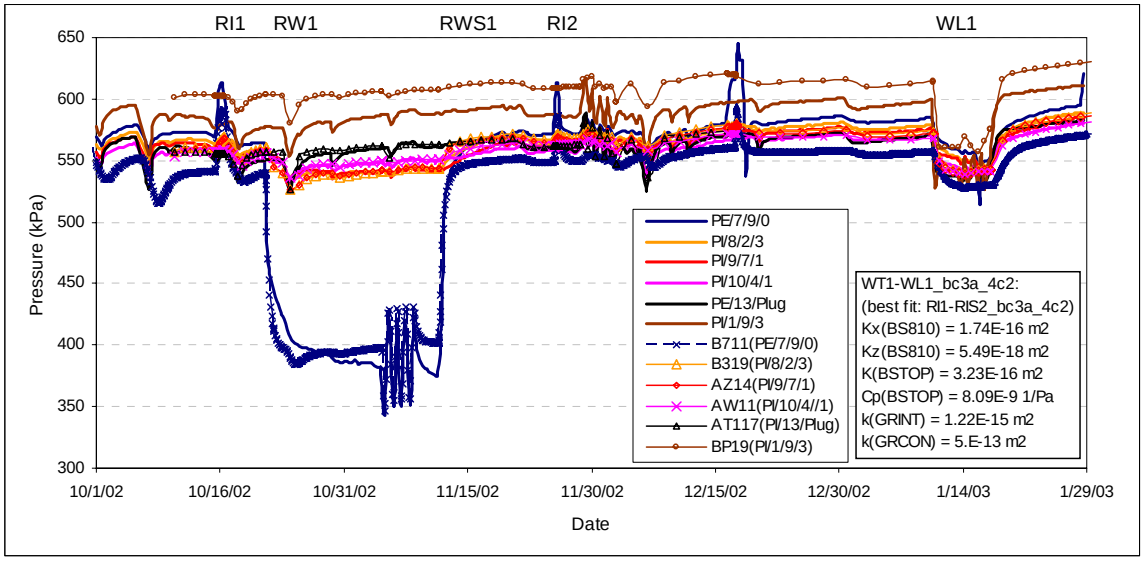

Figure 4 Measurement (lines) and simulation (line with symbols) of the entire WT1 – WL1 sequence using the best-fit parameters from the inverse simulation of WT1 and calibrated permeability for the high-permeability path within the shear zone (GRCON) based on the WL1 response in Layer 1 (solid lines: observed, symbols: computed).

The simulation assuming pressure-dependent permeability of BSTOP produced similar permeabilities for BS810 and a slightly lower permeability for BSTOP (1.09E-16m^2) which then increased linearly by maximum of a factor of 10 over a pressure range from 480 to 560 kPa (Senger, 2005). Thus, both cases suggest a more permeable interface at the top of Layer 8, as represented by BSTOP in the numerical model (Fig. 1). However, the statistical analysis of the inverse simulation did not identify a preferred model.

The permeability estimate for the granite interface (GRINT) from the WT1 response was 1.2E-15 m^2, which is too low to account for the observed hydraulic communication between Layer 1 and the upper cavern during the subsequent WL1 test. Pressure responses in boreholes intersecting the shear zone suggested a separate, high-permeability flow path within the shear zone (GRCON), which was implemented in the model as a separate column of connected elements. The conductance of this flow path was calibrated in a series of forward simulations represented by a permeability of 5.E-13 m^2 (Fig. 4). The simulation indicated an offset of the pressures in Layer 1 (Fig. 4) which can be attributed to the initial pressure distribution which indicated a vertical gradient in the vicinity of the GMT silo which could only be approximated in the numerical model.

Gas Injection Test (RGI1-RGI3b)

The first gas injection phase (RGI1 – RGI3b) consisted of a series of step increases in N_2-gas injection from 1.2 ml(STP)/min to 248 ml(STP)/min (Fig. 2), which were converted to equivalent air-mass flow rates. The variation in water injection rates in the upper cavern was implemented in the numerical model to calibrate the linear permeability decrease of the tunnel seal. A forward simulation assuming constant permeability of the interfaces at the top of Layer 8 (BSTOP) and along the granite (GRINT) based on the WT1 results (Fig. 4) yielded significantly higher pressures during RGI3a and RGI3b. The measured effective stress on the silo top was close to zero at the start of RGI3a, suggesting potential interface opening. The corresponding simulation with calibrated pressure-dependent permeability functions for both the interface at the top of Layer 8 and for the granite interface is shown in Figure 5. For this simulation, the capillary pressure curves for both BS810 and BSTOP were shifted to higher values by increasing the air-entry pressure to account for the higher capillary pressures of the drying curves (Romero and Castellanos, 2004).

At the start of RGI1, the simulated silo pressure is about 23 kPa below the measured silo pressure (Fig. 5) due to the offset in the simulation of WT1–WL1 (Fig. 4). The simulated silo pressure under predicts the observed pressure increase during RGI1 and RGI2a, which is probably caused by non-uniform gas migration in the S/B/Pb layers above the silo, which is not accounted for using the radial mesh. The relative increase associated with RGI2b is reasonably well reproduced and the absolute silo pressures approach the measured pressures (Fig. 5). The pressure-dependent permeability increase for BSTOP was calibrated for a pressure range between 650 and 660 kPa representing potential interface opening. during RGI3a. The subsequent pressure increase during RGI3b required an additional permeability increase along the granite interface (GRINT), which was calibrated for a higher pressure interval between 750 and 760 kPa affecting RGI3b.

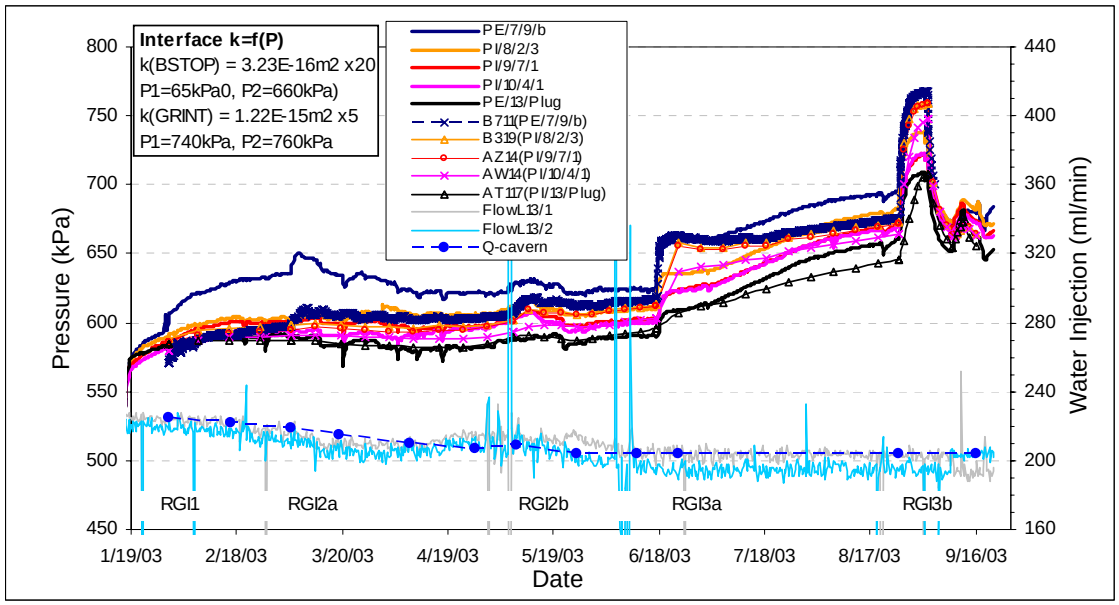

Figure 5 Simulated and measured pressure responses for S/B/Pb sensor during RGI1-RGI3b, also shown is the water injection into the upper cavern (solid lines: observed, symbols: computed).

The simulated silo pressures better reproduced the initial pressure increases during RGI3a and RGI3b. However, the simulated silo pressure increase is lower than that observed following the initially steep increase at the start of RGI3a (Fig. 5). Similarly, the simulation under predicts the gradual increase in the cavern pressure during RGI3a.

The cavern pressure is largely controlled by the water injection into the upper cavern and the apparent change in the tunnel seal permeability. As the gas starts to migrate into the upper cavern, a free gas phase develops in the cavern, causing the cavern pressure to increase. The amount of free gas depends on the quantity of gas that can be dissolved in the pore water and how much gas leaks to the rock and laboratory tunnels. The injected water accounts for dissolved air (corresponding to the solubility equilibrium at atmospheric conditions). Furthermore, the potential leakage of accumulated gas from the top of the cavern is limited to the granite shear zone. No leakage through the top of the tunnel seal is allowed, which facilitates accumulation of the injected gas at the top of the cavern.

The inferred pressure-dependent permeability change during RGI3 no longer strictly corresponds to an effective stress change, because the pressure in the upper cavern (and hence, the total stress in the EBS) increases. However, the pressure-dependent permeability increases along the interfaces may correspond changes in the minimum effective stress at the top of the silo and minimum horizontal stress at the granite interface, based on coupled hydro-mechanical modeling results using Code Bright (Alonso et al., 2005).

The simulated distribution of gas saturation and gas flow (left diagram) and pressure, and water flow (right diagram) during the gas injection phase (Fig. 6) indicates the migration of the gas from the silo into the overlying sand/bentonite, and then into the upper cavern. At the start of RGI1, there is some small amount of remaining air in the overlying S/B/Pb layers in addition to the unsaturated conditions in the S/B layers (Fig. 6).

The onset of gas migration into the sand/bentonite corresponds to the peak pressure during RGI2a. Gas migration is not limited to the interface (BSTOP) above the silo, but extends into the S/B/Pb layer above (BSTOP), because of some remaining air. At the end of RGI2b, the gas front reaches the base of the upper cavern along the granite interface (GRINT). The subsequent increase in the gas injection rate at the start of RGI3a shows a significant increase in silo pressure and cavern pressure (Fig. 5) corresponding to the development of free gas in the upper cavern (Fig. 6).

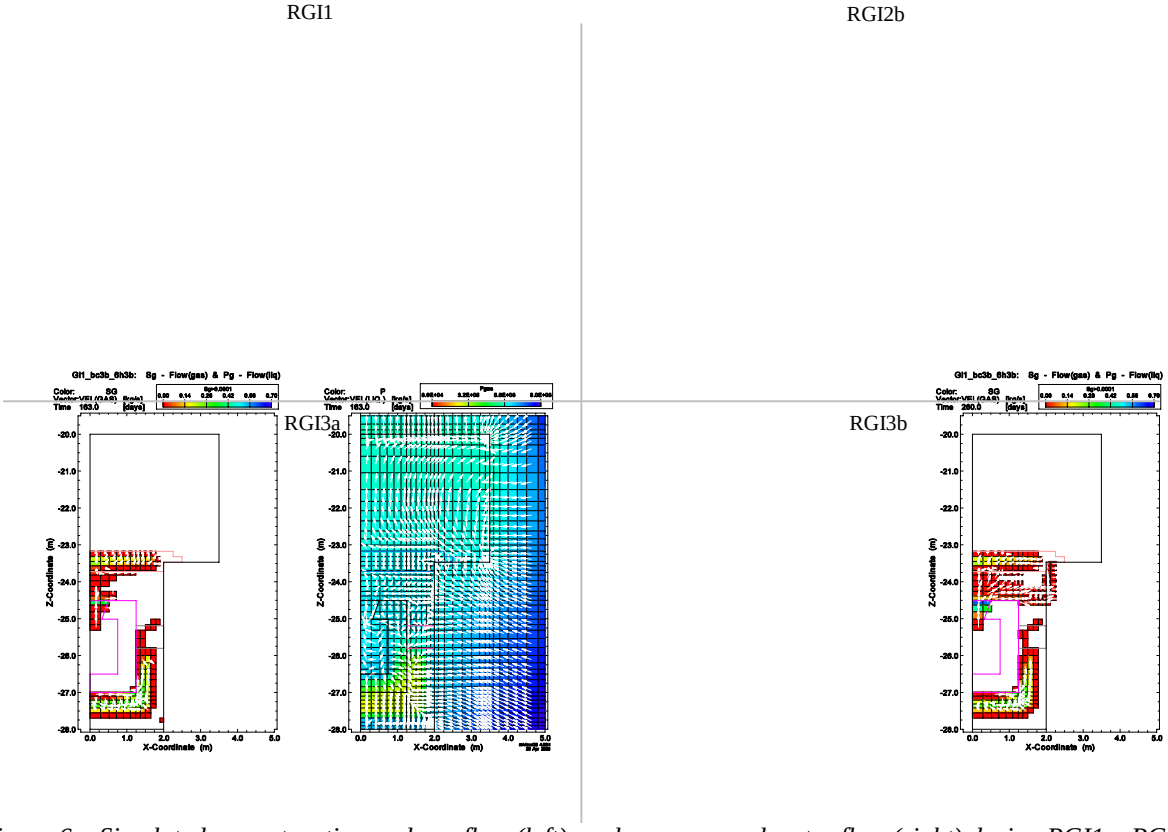

Figure 6 Simulated gas saturation and gas flow (left), and pressure and water flow (right) during RGI1 – RGI3b

The simulated saturations at grid elements corresponding to selected TDR sensors are converted to water content based on a porosity of 0.28 for the S/B/Pb Layers 8 - 10 (Fig. 7). The measured water content data from the TDR sensors should be used to compare the relative changes in water content rather than the absolute magnitude, because of uncertainty in the TDR calibrations and in porosity near the sensors. The results indicate that temporal changes in saturation compare reasonably well with the measured changes in water content during RGI1-RGI3b, supporting the simulated gas migration pattern shown in Figure 6.

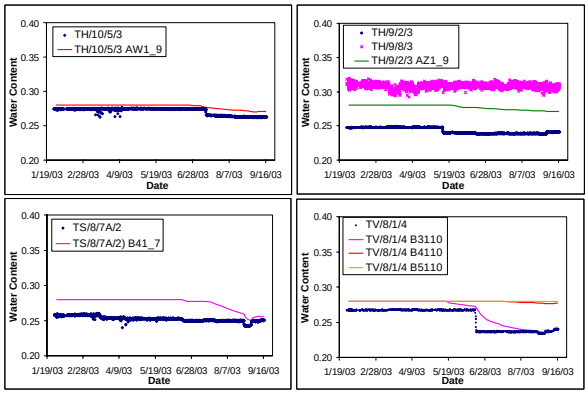

Figure 7 Comparison of simulated (lines) and measured (symbols) water content at selected TDR sensor during RGI1-RGI3b.

Water Test 2 and Second Gas Injection Phase

The first gas injection phase was followed by a recovery period including a constant-rate water injection at the top of the upper cavern (UCV-RI1), a reduction in water injection into the upper cavern, and removal of gas from the silo, vent, and from selected PE lines (Fig. 2).

The second water test (WT2) included the same test sequences used for WT1 (i.e., CVSin1, RI1, RW1, RI2, and UCV-RI1) to characterize potential changes in hydraulic properties of the sand/bentonite. For the second gas injection phase (Stage 7) following WT2, gas was injected at two different rates: (a) 2.5 ml(STP)/min (RGI4a), and (b) 50 ml(STP)/min (RGI4b-c).

During the recovery phase prior to WT2, the same linear decrease of the tunnel seal permeability used during the preceding gas injection phase could not reproduce the observed cavern pressure during WT2. Rather, the reduction in water injection and associated pressure decline suggested a greater permeability reduction, which was implemented by reducing the tunnel seal permeability at the start of the simulation. This produced a significant perturbation in simulated pressure at the start, which dissipated by the start of WT2 reproducing the observed cavern pressure reasonably well during WT2 and subsequent gas injection phase (Fig. 8).

The analysis of the pressure responses of the different WT2 sequences indicated a noticeable decrease in the overall permeability of the S/B/Pb layers. This was accounted for by reducing the horizontal and vertical permeability for BS810 to 1.E-17 m^2 and 1.E-18 m^2, respectively, which corresponds well with in situ permeability measurements and measured water permeability from block samples taken during the dismantling of the EBS (Romero and Castellanos, 2006). Similarly, the vertical permeability of BSTOP was decreased to 1.E-18m^2, whereas the horizontal permeability was only reduced to 1.E-16m^2. A reduction to only 1.E-17m^2 resulted in a noticeably offset of the simulated silo pressure, suggesting a higher permeability is required for BSTOP compared to that for BS810.

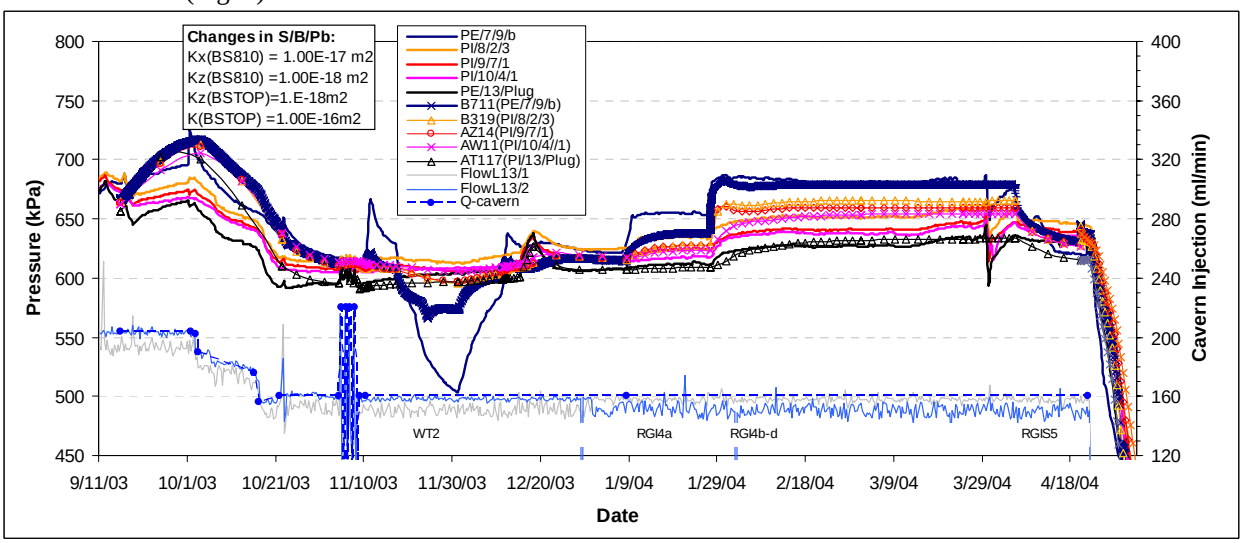

Figure 8 Simulated and measured pressure responses for S/B/Pb sensor during WT2 – RGI4, also shown is the water injection into the upper cavern (solid lines: observed, symbols: computed).

The simulated pressure response of the WT2 sequence (Fig. 8) is greatly affected by the previously injected gas during Stage 4, which in the models accumulated preferentially in the interface layer (BSTOP) at the top of the silo and in the silo vent (Fig. 6). As a result, the simulation under predicts the pressure buildup and drawdown during the injection and withdrawal events, respectively (Fig. 8). Moreover, the simulation of the second gas injection phase also produced lower pressures during RGI4a compared to the observed step increase. The subsequent step increase at the start of RGI4b is well reproduced in the model (Fig. 8). The near constant pressure response during RGI4b is reproduced assuming a constant permeability for the interface at the top of the silo and for the granite interface. The simulated increase in the cavern pressure at the start of RGI4b indicates gas flow into the upper cavern. In the current simulation, preferential gas migration still occurs along the interface layer due to relatively high gas saturation along the top of Layer 8 and along the granite interface. In previous modeling, the simulation of RGI4 indicated "re-opening" of the granite interface at lower pressures, corresponding to that inferred from the RGI3b response. Both scenarios can reproduce the RGI4 response reasonably well, depending on the assumed capillary pressures curves for the S/B/Pb buffer which indicated a significant decrease in permeability.

The overall gas volume in the upper cavern in the simulation is compared to that inferred from compressibilities estimated from test responses, which show a good agreement during RGI3b and early part of WT2 but is somewhat higher at the end of WT2 and at the end of RGI4 (Fig. 9).

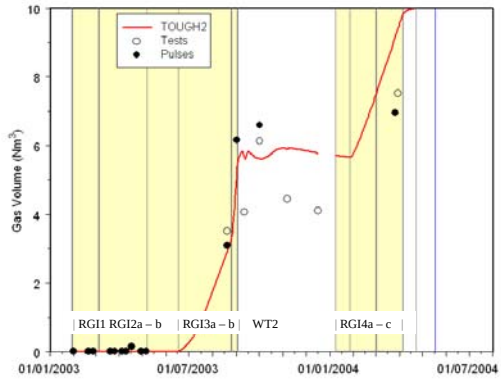

Figure 9 Simulated gas accumulation (as m^3 STP) in the upper cavern, compared to estimates from test responses.

CONCLUSIONS

The GMT experiment produced complex two-phase flow behavior and apparent coupled hydromechanical phenomena associated with gas migration through the sand/bentonite buffer material. However, the EBS responses indicated close interaction with the surrounding geosphere affecting the water inflow from the upper cavern to the tunnel through the tunnel seal and the shear zone and escape of gas from the upper cavern. The results of the numerical modeling of the GMT experiment show that the main features and processes of the different stages of the experiment could be reasonably well reproduced in a design model using the two-phase flow code TOUGH2. Several issues require further investigation including i) the offset between silo pressure and that in the upper cavern and the sand/bentonite and ii) the observed permeability decrease of the sand/bentonite buffer, which may be caused by compaction associated with the pressure decline following the first gas test. Further insight on the gas migration could be obtained from the analysis of the multiple gas tracer responses during RGI4 which are not yet fully interpreted.

ACKNOWLEDGMENT

This study has been performed under funding from the Ministry of Economy, Trade and Industry (METI) in Japan.

REFERENCES

Alonso, E., and Olivella, S., Delahaye, C., GMT/IR 04-04: Modeling the hydromechanical behaviour of GMT in-situ test including interface elements. Nagra Project Report 05-05, Wettingen, CH, 2005

Finsterle, S., ITOUGH2 User's Guide, Report LBNL-40040 Lawrence Berkeley National Laboratory, Berkeley, Calif., 1999.

Pruess, K, TOUGH2 – A general-purpose numerical simulator for multiphase fluid and heat flow, Report LBL-29400, Lawrence Berkeley Laboratory, Berkeley, Calif., 1991.

Romero, E., Garcia, I., Alonso, E., GMT/IR 02-02: Laboratory tests on compacted sand/bentonite buffer material used in the GMT in-situ emplacement, Nagra Project Report 03-03, Wettingen, CH, 2003.

Romero, E., and Castellanos, E., GMT/IR 03-03: Complementary tests on compacted sand/bentonite/lead/nitrate buffer material for the GMT Emplacement Project. Nagra Project Report 04-07, Wettingen, CH, 2004,

Romero, E., and Castellanos, E., 2006, Tests on in-situ sand/bentonite buffer material. UPC report.

Senger, R.K., GMT/IR 04-03: TOUGH2 Design modeling for the GMT Experiment (FY2004). Nagra Project Report 05-04, Wettingen, CH, 2005.

Shimura, T., A. Fujiwara, S. Vomvoris, P. Marschall, B. Lanyon, K. Ando, S. Yamamoto, Large-Scale Gas Migration Test at Grimsel Test Site, in Proceedings, IHLRWM Conference, Las Vegas, Nevada, 2006.